



# Effects of Illuminance Intensity on the Green Channel of Remote Photoplethysmography (rPPG) Signals

Saygun Guler<sup>1\*</sup>, Ozberk Ozturk<sup>1</sup>, Ata Golparvar<sup>1,2</sup>, Huseyin Dogan<sup>3</sup> and Murat Kaya Yapici<sup>1,4</sup>

<sup>1\*</sup>Department of Electronics Engineering, Faculty of Engineering and Natural Sciences, Sabanci University, Tuzla, Istanbul, 34956, Turkey.

<sup>2</sup>Integrated Circuits Laboratory (ICLAB), École Polytechnique Fédérale de Lausanne (EPFL), Neuchâtel, 2002, Switzerland.

<sup>3</sup>Department of Computing and Informatics, Bournemouth University, Fern Barrow, Bournemouth, BH12 5BB, Dorset, United Kingdom.

<sup>4</sup>Department of Electrical Engineering, University of Washington, 98195, Washington, USA.

\*Corresponding author(s). E-mail(s):

[saygun.guler@sabanciuniv.edu](mailto:saygun.guler@sabanciuniv.edu);

Contributing authors: [ozberk@sabanciuniv.edu](mailto:ozberk@sabanciuniv.edu);

[ata.golparvar@epfl.ch](mailto:ata.golparvar@epfl.ch); [hdogan@bournemouth.ac.uk](mailto:hdogan@bournemouth.ac.uk);

[murat.yapici@sabanciuniv.edu](mailto:murat.yapici@sabanciuniv.edu);

## Abstract

Point-of-care remote photoplethysmography (rPPG) devices that utilize low-cost RGB cameras have drawn considerable attention due to their convenience in contactless and non-invasive vital signs monitoring. In rPPG, sufficient lighting conditions are essential for obtaining accurate diagnostics by observing the complete signal morphology. The effects of illuminance intensity and light source settings play a significant role in rPPG assessment quality, and it was previously observed that different lighting schemes result in different signal quality and morphology. This study presents a quantitative empirical analysis where

047 the quality and morphology of rPPG signals were assessed under dif-  
048 ferent light settings. Participants' faces were exposed to the white LED  
049 spotlight, first when the sources were installed directly behind the  
050 video camera, and then when the sources were installed in a cross-  
051 polarized scheme. Hence, the effect of specular reflectance on rPPG  
052 signals could be observed in an increasing projection. **The signal quali-**  
053 **ties were analyzed in each intensity level using a signal-to-noise (SNR)**  
054 **ratio metric. In 3 of 7 participants, placing the video camera on the**  
055 **same level as the light source led to signal quality loss of up to 3**  
056 **dB for the range 30-60 Lux. In addition, two fundamental morpho-**  
057 **logical features were analyzed, and the derivative-related feature was**  
058 **found to be increasing with illuminance intensity in 6 of 7 participants.**

059 **Keywords:** remote photoplethysmography (rPPG), vital signs  
060 measurements, heart rate, digital health, health-care applications

## 061 062 063 1 Introduction

064  
065 Advancements in mobile technologies have led to a new era in transferring  
066 and processing a wide range of data types [Abd Elaziz et al \(2021\)](#); [Attiya](#)  
067 [et al \(2022\)](#). Integration with smart devices facilitated access to healthcare ser-  
068 vices [Acar et al \(2019\)](#). Recent advancements in image processing have made  
069 the extraction of vital signs from remote, contactless, photoplethysmographic  
070 (rPPG) signals possible [Rouast et al \(2018\)](#). The fundamental principle gov-  
071 erning rPPG is similar to that of contact PPG; they both exploit the light  
072 absorption differences of oxygenated and deoxygenated hemoglobin in capil-  
073 lary blood vessels [Kamshilin and Margaryants \(2017\)](#). While PPG primarily  
074 uses visible and near-infrared light sources, rPPG merely acquires visible wave-  
075 length as modern video cameras compose images in the RGB color channels  
076 [Sun and Thakor \(2016\)](#); [Allen \(2007\)](#). The rPPG measures the blood that  
077 circulates through the facial capillaries in every heartbeat resulting in imper-  
078 ceptible color variations on the skin, and modern video cameras can capture  
079 those variations under sufficient ambient conditions. It has been previously  
080 shown that the green channel has the most robust pulse information amongst  
081 the three RGB channels since the hemoglobin absorption is at its highest under  
082 green light [Verkruysse et al \(2008\)](#). This is the main reason why we attempted  
083 to investigate the effects only on the denoised green channel.

084  
085 Different methods have been proposed for generating pulse signals in rPPG.  
086 These methods have recently been classified under three subsections as design-  
087 based, model-based, and blind source separation methods [Sinha et al \(2020\)](#).  
088 Design-based methods involve the algorithms where the spatial representation  
089 is redefined, and they usually do not require a priori information of skin tone  
090 or illuminant [Eaton et al \(2018\)](#); [Xu et al \(2014\)](#). However, they are mostly  
091 dependent on the number of pixels in the region of interest (ROI) mask [Wang](#)  
092 [et al \(2016b\)](#). Model-based methods, on the other hand, are very useful for

motion robustness [de Haan and van Leest \(2014\)](#). Chrominance-based method (CHROM) was introduced which builds two orthogonal chrominance signal components (X,Y); then it generates the pulse signal as combinations of X,Y [de Haan and Jeanne \(2013\)](#). Blind source separation methods are also effective when the original RGB signals are contaminated with noise or motion artifacts. Their principle is to exploit the signals as statistical data sets rather than to process them in a time or a frequency domain directly. JADE-ICA algorithm was successfully implemented in rPPG for heart rate (HR) predicting with 12 participants [Poh et al \(2010\)](#). Later, component analysis techniques were improved and tailored in rPPG applications for better accuracy [Tsouri et al \(2012\)](#); [Macwan et al \(2019\)](#). However, in cases where subjects have less or no motion at all, there is usually no need to use source separation methods for heart rate estimation as the raw signals have already sufficient pulse information.

The quality of an rPPG signal depends on several things such as illuminance level, type of camera lenses, skin type, skin color, environmental conditions, and make up [Wang and Shan \(2019\)](#). However, it is essential to consider the principles of skin reflection properties prior to collecting data for measurements. Wang et al. described the skin reflection model in detail and explained how the pulsatile information could be interpreted mathematically as depicted in Figure 1 [Wang et al \(2016a\)](#). Their analysis was purely based on the dichromatic reflection model [Tominaga \(1994\)](#). The skin pixels of RGB channels were defined as a time-varying function as in Equation 1;

$$C_k(t) = I(t) * [v_s(t) + v_d(t)] + v_n(t) \quad (1)$$

where  $I(t)$  represents the luminance intensity,  $v_s(t)$  represents the specular reflection,  $v_d(t)$  represents the diffuse reflection, and  $v_n(t)$  represents the noise induced by the camera sensor. The specular reflection phenomenon was described as a mirror-like effect which has no pulsatile information whatsoever. However, diffuse reflection is directly related to the light absorption of the skin, and it contains information regarding blood volume changes.

Light variance is one of the common challenges in rPPG and researchers have attempted to improve light tolerance with different methods. Jeanne et al. presented a method using infra-red reference light for remote HR measurements where the ambient light conditions are highly dynamic [Jeanne et al \(2013\)](#). Li et al. implemented an adaptive least mean square filter in their algorithm to reduce the noise induced by light variation for HR measurements [Li et al \(2014\)](#). Tulyakov et al.'s method calculates the HR while simultaneously determining suitable ROI depending on the environmental conditions such as motion or illumination variation [Tulyakov et al \(2016\)](#). Wu et al. proposed a neural network-based method for denoising pulse signals of a driver under ambient traffic lights [Wu et al \(2019\)](#). In addition to the techniques proposed to overcome those challenges regarding light conditions, Blackford et al. proposed a spectroscopy analysis to investigate the spectral properties of blood volume pulses [Blackford et al \(2018\)](#).

139  
 140  
 141  
 142  
 143  
 144  
 145  
 146  
 147  
 148  
 149  
 150  
 151  
 152  
 153  
 154  
 155  
 156  
 157  
 158  
 159  
 160  
 161  
 162  
 163  
 164  
 165  
 166  
 167  
 168  
 169  
 170  
 171  
 172  
 173  
 174  
 175  
 176  
 177  
 178  
 179  
 180  
 181  
 182  
 183  
 184

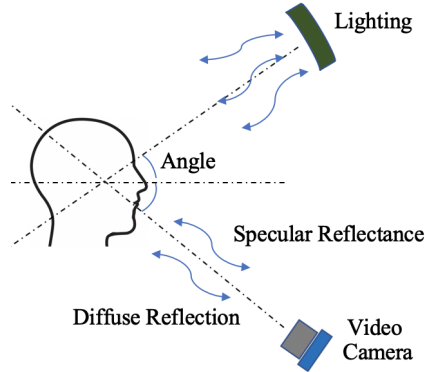


**Fig. 1:** Skin Reflection Model explains the reflection properties of skin, and it helps to justify the pulsatile information extracted from rPPG.

One of the significant effects of light variance is on rPPG pulse morphology. Unlike the conventional PPG, rPPG signals do not have a characteristic pulse morphology as it varies according to several factors (e.g., lighting, sensor, recording device). This situation calls some of the vital signs measurements in question (i.e., blood pressure [BP]). Especially for BP measurements, an accurate feature extraction process is essential when training the artificial neural networks being used Luo et al (2019). The studies published so far do not prove that the rPPG features are reliable enough to be fed into the neural networks for running solid health applications/algorithms. This is one of the main reasons why all aspects of the rPPG signal morphology must be studied thoroughly; the ambient light conditions (light settings, light intensity), subject's skin tone (as this may have an effect on the reflectivity, which is related to the quality of the pulsatile information taken from the rPPG measurement), and skin conditions (cleanness, oil, make-up, local melanin variations, etc.).

Several physiological models have been proposed in cPPG to explain the light interaction in reflective photoplethysmography Kamshilin and Margaryants (2017). While each model has its own advantages in justifying the signal morphology and behavior, more empirical analyses are needed for hypothesizing similar models in rPPG-based sensing applications. The findings in this study, therefore, are essential to find the answers of the following questions; (1) How does the illuminance intensity affect the rPPG signal quality? (2) Does the illuminance intensity affect the morphological features in rPPG, and if so, to what extent and what are the associated experimental challenges?

Although there are studies associated with the effects of light intensity variations on PPG signals, this is the first attempt to quantify the signal quality under different illuminance intensities systematically. We established two experimental setups and analyzed the illuminance intensity effects on 42 rPPG recordings with a signal quality metric and two morphological features.

## 2 Methods

### 2.1 Experimental Setup & Participants

The experiments were carried out in the physiology laboratory in Bournemouth University (BU) where the Research Panel of BU approved the study. Seven Caucasian volunteers aged between 24 and 38 participated in the study. Darker skin tones are excluded for this trial as they require different biases and assumptions when processing rPPG signals Nowara et al (2020). The informed consent of each participant was obtained prior to the sessions. They were priorly requested not to wear make-up as such a factor requires additional assumptions and knowledge such as the type or quantity of the material that covered the specific parts of the face Wang and Shan (2019).

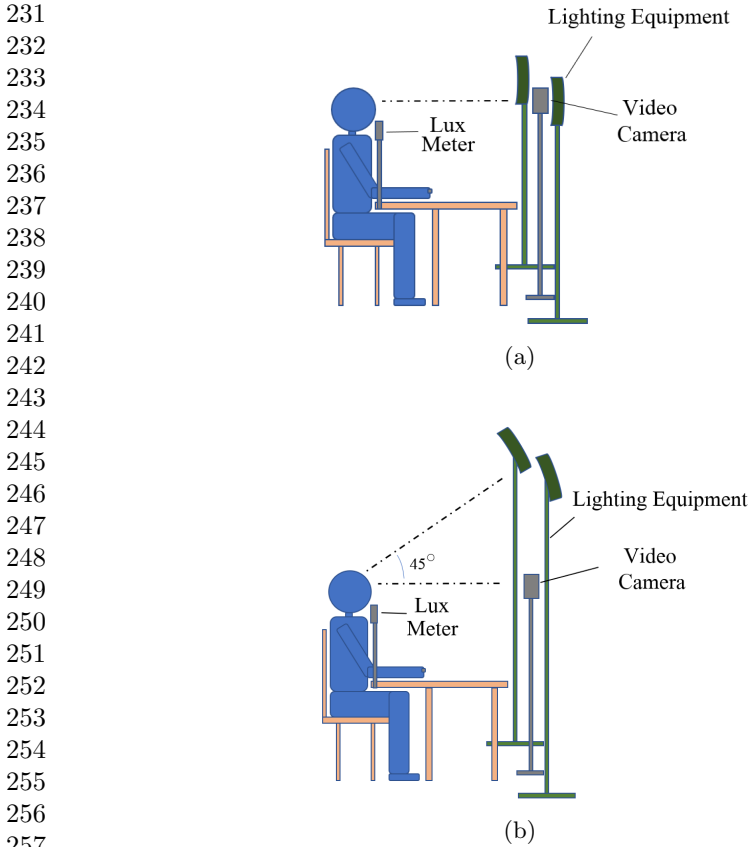
First, the subjects' faces were exposed to 30-60-100 lux respectively in a direct scheme as shown in Figure 2a; then they were exposed to 60-90-130 lux in a cross-polarized scheme as shown in Figure 2b. The illuminance ranges were so selected because our empirical pre-studies had shown that those lux levels would not irritate and induce discomfort to the human eye under those settings.

Controlled lighting equipment (Neewer 480 LED Panel Light) was used as the illuminant source. Illuminance was measured with a lux meter installed directly in front of the participant's face (Urceri MT-912 Light Meter). The RGB video camera was a CCD Sony DSCH300, and it was stabilized on an adjustable tripod. No additional lenses were attached, and no artificial effects were used. The distance between the participant and lighting equipment was 70 cm. The position of the equipment was so arranged that the regions of interest were not exposed to any potential shadow fall induced by the rays of light. As Kwon et al. and Lempe et al.'s analyses showed that the best ROI for spatial averaging is the cheeks, we manually created ROI masks for each participant Lempe et al (2013); Sungjun Kwon et al (2015). Participants were asked to keep as still as possible throughout the sessions. The recordings were taken in 30 frames per second, and video lengths were 30 seconds for each illuminance level.

### 2.2 Signal Analysis

All signal processing operations were carried out in custom-written scripts in MATLAB (MathWorks, Natick, Massachusetts, USA). The rPPG pulse data were presented as the normalized green channel only by taking the spatial average of the ROI pixels in every frame. This can be formalized as in the Equation 2 where  $\mu(G_i)$  is the spatial mean in time domain. The multiplication of -1 is due to the need for inverting the signal as the *video camera rPPG* exhibits a reflectance oximetry behaviour, and it needs to be flipped over after normalization. In order to observe the morphological changes, a 3rd order Savitzky-Golay filter was used because of its better transient capturing properties for removing high frequency components from all the signals.

185  
186  
187  
188  
189  
190  
191  
192  
193  
194  
195  
196  
197  
198  
199  
200  
201  
202  
203  
204  
205  
206  
207  
208  
209  
210  
211  
212  
213  
214  
215  
216  
217  
218  
219  
220  
221  
222  
223  
224  
225  
226  
227  
228  
229  
230



258 **Fig. 2:** In direct scheme (a), video camera and lighting were in the same  
259 horizontal plane. In cross-polarized scheme (b), 45 degree was set between the  
260 camera and lighting.

261  
262  
263  
264  
265  
266  
267  
268  
269  
270  
271  
272  
273  
274  
275  
276

$$G_n = -1 * \frac{G_i}{\mu(G_i)} \quad (2)$$

We have implemented De Haan et al.'s signal-to-noise ratio (SNR) metric to assess the usability and quality of rPPG signals [de Haan and Jeanne \(2013\)](#). The 30-second filtered temporal datasets were assessed in frequency domain. This method calculates the energy around the harmonics and remaining portion in the power spectrum; then an SNR score in dB is presented by taking the ratio of both. Signal and noise calculations are formulated as in Equation [3](#) and [4](#) where  $S(f)$  represents the spectrum and  $U_t(f)$  represents the binary template.

$$Signal = \sum_{f=0.2}^{15} (U_t(f)S(f)) \quad (3)$$

$$Noise = \sum_{f=0.2}^{15} ((1 - U_t(f))(S(f))) \quad (4)$$

$$SNR\ score = 10 \log_{10} \left( \frac{Signal}{Noise} \right) \quad (5)$$

Since all the participants were asked to keep as still as possible during the recordings, the predictions extracted from the frequency domain were consistent and the spectra were clean.

### 3 Results

Pulse signal qualities were assessed using the SNR metric to see the illuminance intensity effect on rPPG signals. The SNR scores of the normalized green channel are presented in Figures 3a and 3b.

Beside the signal quality, the two main features of the rPPG signals were analyzed to observe the change in morphology in the normalized green channel. The first feature is the time in seconds between the maxima of the first derivative of the pulse signal (where it rises rapidly) and the crest point. This is shown with a participant image in Figure 4 as “Length A.” The second feature, on the other hand, is simply the amplitude of the pulse signal; it is the distance in y axis between the start and crest points of the pulse. This is shown as “Length B.” Signal morphology analyses were made by detecting each pulse in the time domain. The values presented in tables are the mean values of the features extracted from each pulse in 30-second recordings. Standard deviation (SD) for the pulse amplitude in each intensity level was within the range of 0.1-0.2, and SD for the time between the maxima of the first derivative of the pulse signal and the crest point was within the range of 0.01-0.1. The only linearity observed in morphology analyses was in the distance between the maxima of the first derivative of the pulse signal and crest point. In 6 participants, the feature “Length A” increased with the illuminance intensity as can be followed in Table 1. The pulse amplitude did not exhibit a linearity in distance between the start and crest points of the pulse (Length B) in any case whatsoever. However, in the cross-polarized scheme, the amplitudes have been shown to vary by up to 0.1 (RGB colour unit), and in direct scheme, they have been shown to vary by up to 0.13 (RGB colour unit) in the y axis.

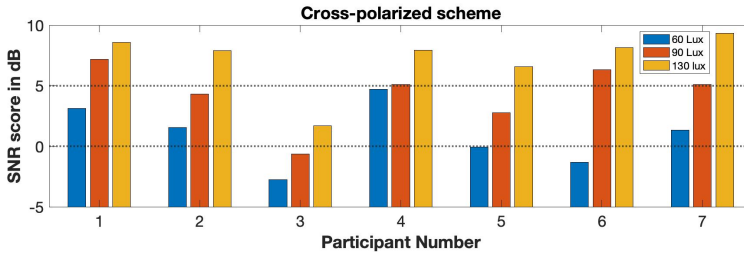
### 4 Discussion

The prevailing opinion in remote measurements is that “the illuminance intensity will affect the rPPG assessment positively”, however, our results have

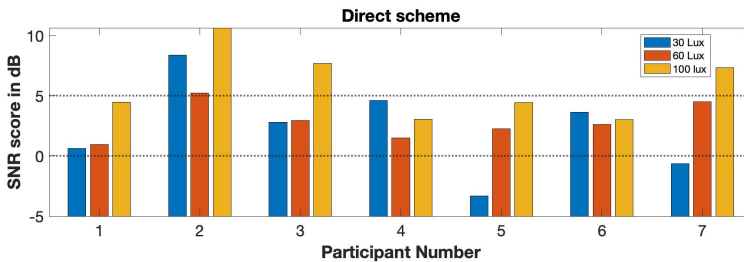
277  
278  
279  
280  
281  
282  
283  
284  
285  
286  
287  
288  
289  
290  
291  
292  
293  
294  
295  
296  
297  
298  
299  
300  
301  
302  
303  
304  
305  
306  
307  
308  
309  
310  
311  
312  
313  
314  
315  
316  
317  
318  
319  
320  
321  
322

8 *Effects of Illuminance Intensity*

323 shown that this notion is likely to be refuted when the video camera is placed  
 324 within the same horizontal direction as the light source. The effect of the light  
 325 setting in the direct scheme where there is zero angle between the light source  
 326 and video capturing device, might reduce the usability of the rPPG signals.  
 327 Figure 3b shows how such an inappropriate setup design could introduce an  
 328 unpredictability in the pulse signal quality where high illuminance increased  
 329 the mirror-like effect in 3 of the participants.



(a)



(b)

352 **Fig. 3:** SNR scores of the green channel in cross-polarized scheme form an  
 353 increasing projection in all participants (a). When the video camera and light  
 354 source are in the same horizontal plane with no angle, SNRs exhibited an  
 355 unpredictability in 3 participants (b).

356

357

358

359

360

361

362

363

364

365

366

367

368

The SNR analyses have shown that the readability of the pulsatile information increases with higher illuminance intensity where the illuminant is set up in a cross-polarized scheme. When there is no angle between the illuminant and the video recording device (i.e., direct scheme), the mirror-like phenomenon of the skin-light interaction (i.e., specular reflectance) engenders a signal quality loss and this potentially might lead to an inaccurate rPPG assessment in which case an advanced algorithm can be implemented to the application [Jeanne et al \(2013\)](#). Though the sample size was small in this trial, these findings show that the raw signal morphology concept needs more detailed spectroscopy studies



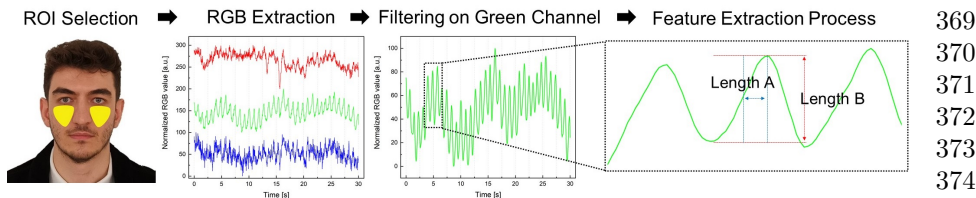


**Fig. 4:** Once the RGB channel data were extracted from the same region in all participants, the green channel was filtered with a smoothing Sav-Gol. Finally, morphological features were extracted.

	Cross-Polarized Scheme			Direct Scheme		
	60 Lux	90 Lux	130 Lux	30 Lux	60 Lux	100 Lux
Participant 1	0.1836	0.2266	0.1946	0.1941	0.2395	0.196
Participant 2	<b>0.1891</b>	<b>0.2377</b>	<b>0.2753</b>	0.1768	0.2378	0.2108
Participant 3	<b>0.2219</b>	<b>0.2267</b>	<b>0.2472</b>	0.2381	0.2079	0.2213
Participant 4	<b>0.3161</b>	<b>0.3233</b>	<b>0.3596</b>	0.3587	0.2709	0.2834
Participant 5	<b>0.2261</b>	<b>0.2229</b>	<b>0.244</b>	0.1202	0.2454	0.1883
Participant 6	<b>0.167</b>	<b>0.1756</b>	<b>0.1905</b>	0.2209	0.1908	0.1966
Participant 7	<b>0.216</b>	<b>0.2451</b>	<b>0.2706</b>	0.2377	0.2617	0.2482

**Table 1:** Average Length A. The time in seconds between the maxima of the first derivative of the pulse signal and the crest point.

to improve understanding of the rPPG theory better. The factors to be investigated might be the types of camera (whether it is an RGB color model or not), and the color sensors embedded in the recording device (CCD, CMOS or a combination of those technologies). The major limitation in our study, on the other hand, was the illuminance intensity range. Safety was an important matter, and it was decided not to risk causing any eye discomfort to the participants. However, with light-blocking glasses, the study can be extended in the future with different light wavelengths. Also, the sample size could be extended including darker skin tones. **It is still not clear that if rPPG features carry vital information about blood pressure as cPPG features do Rong and Li (2021). We expect this study to initiate a trend in which morphological features are deeply investigated from the spectroscopic and light intensity aspects.**

## 5 Conclusion

Remote photoplethysmography (rPPG) signals carry vital information about human cardiovascular dynamics. Here, we investigated how the green channel in rPPG reacts to illuminance intensity change in the ranges 30-60-90 and 60-90-130 lux. We reported signal qualities in SNR metric and analyzed the morphological changes by observing the two main features of photoplethysmography signals in two different experimental setups. **It was hypothesized that the**

415 specular reflectance leads to signal quality loss in rPPG signals, and we found  
416 that in the range of 60-130 lux, which is considered to be low level in compari-  
417 son with a typical office environment, illuminance intensity can affect the SNR  
418 up to 7 dB. The derivative-related morphological feature, on the other hand,  
419 was observed to vary up to 0.1 (RGB color unit) in both settings. Additionally,  
420 linearity was observed when the light setting was in a cross-polarized scheme.  
421 This study confirms that the placement of light sources significantly affects  
422 rPPG assessments and must be carefully considered when designing such an  
423 application in rPPG. The results encourage us to propose more detailed stud-  
424 ies to determine the best pulse generation methods in various environmental  
425 conditions and ambient settings to get an accurate rPPG assessment. In future  
426 works, we plan to extend the study where more volunteers from multiple back-  
427 grounds are recruited, especially females and the elderly. Thus we will be able  
428 to investigate not only the effects of skin homogeneity but also the skin color  
429 on rPPG signals as well.

430

## 431 **6 Statements and Declarations**

432

433 This study was partially funded by the Sabanci University research fund.

434

435 **Conflict of Interest.** The authors declare no conflicts of interest.

436

437 **Ethical approval.** The experiments were conducted in Bournemouth Uni-  
438 versity (BU) and The Research Ethics Panel of BU approved the study which  
439 was performed in accordance with the ethical standards as laid down in the  
440 1964 Declaration of Helsinki and its later amendments.

441

442 **Consent to participate.** The informed consent of each participant was  
443 obtained prior to the sessions. The authors affirm that all participants provided  
444 informed consent for publication of the images and relevant data that were  
445 collected during the experiments.

446

## 447 **References**

448

449 Abd Elaziz M, Abualigah L, Ibrahim RA, et al (2021) IoT Workflow Schedul-  
450 ing Using Intelligent Arithmetic Optimization Algorithm in Fog Computing.  
451 Computational Intelligence and Neuroscience 2021:1–14. <https://doi.org/10.1155/2021/9114113>, URL <https://www.hindawi.com/journals/cin/2021/9114113/>

452

453 Acar G, Ozturk O, Golparvar AJ, et al (2019) Wearable and Flexible Tex-  
454 tile Electrodes for Biopotential Signal Monitoring: A review. Electronics  
455 8(5):479. <https://doi.org/10.3390/electronics8050479>, URL <https://www.mdpi.com/2079-9292/8/5/479>

456

457 Allen J (2007) Photoplethysmography and its application in clinical physiolog-  
458 ical measurement. Physiological Measurement 28(3):R1–R39. <https://doi.org/10.1088/0967-0486/28/3/R01>

459

460

- [org/10.1088/0967-3334/28/3/R01](https://doi.org/10.1088/0967-3334/28/3/R01), URL <http://stacks.iop.org/0967-3334/28/i=3/a=R01?key=crossref.71c24bedf5376f8de1a8ea975615500b> 461  
462  
463
- Attiya I, Abualigah L, Elsadek D, et al (2022) An Intelligent Chimp Optimizer for Scheduling of IoT Application Tasks in Fog Computing. *Mathematics* 10(7):1100. <https://doi.org/10.3390/math10071100>, URL <https://www.mdpi.com/2227-7390/10/7/1100> 464  
465  
466  
467  
468
- Blackford EB, Estep JR, McDuff DJ (2018) Remote spectral measurements of the blood volume pulse with applications for imaging photoplethysmography. In: Coté GL (ed) *Optical Diagnostics and Sensing XVIII: Toward Point-of-Care Diagnostics*. SPIE, San Francisco, United States, p 41, <https://doi.org/10.1117/12.2291073>, URL <https://www.spiedigitallibrary.org/conference-proceedings-of-spie/10501/2291073/Remote-spectral-measurements-of-the-blood-volume-pulse-with-applications/10.1117/12.2291073.full> 469  
470  
471  
472  
473  
474  
475  
476  
477
- Eaton A, Vishwanath K, Cheng CH, et al (2018) Lock-in technique for extraction of pulse rates and associated confidence levels from video. *Applied Optics* 57(16):4360. <https://doi.org/10.1364/AO.57.004360>, URL <https://www.osapublishing.org/abstract.cfm?URI=ao-57-16-4360> 478  
479  
480  
481  
482
- de Haan G, Jeanne V (2013) Robust Pulse Rate From Chrominance-Based rPPG. *IEEE Transactions on Biomedical Engineering* 60(10):2878–2886. <https://doi.org/10.1109/TBME.2013.2266196>, URL <https://ieeexplore.ieee.org/document/6523142/> 483  
484  
485  
486
- de Haan G, van Leest A (2014) Improved motion robustness of remote-PPG by using the blood volume pulse signature. *Physiological Measurement* 35(9):1913–1926. <https://doi.org/10.1088/0967-3334/35/9/1913>, URL <http://stacks.iop.org/0967-3334/35/i=9/a=1913?key=crossref.f46064b855e94d2d426c3c66e22da0ba> 487  
488  
489  
490  
491  
492
- Jeanne V, Asselman M, den Brinker B, et al (2013) Camera-based heart rate monitoring in highly dynamic light conditions. In: 2013 International Conference on Connected Vehicles and Expo (ICCVE). IEEE, Las Vegas, NV, USA, pp 798–799, <https://doi.org/10.1109/ICCVE.2013.6799899>, URL <http://ieeexplore.ieee.org/document/6799899/> 493  
494  
495  
496  
497  
498
- Kamshilin AA, Margaryants NB (2017) Origin of Photoplethysmographic Waveform at Green Light. *Physics Procedia* 86:72–80. <https://doi.org/10.1016/j.phpro.2017.01.024>, URL <https://linkinghub.elsevier.com/retrieve/pii/S187538921730024X> 499  
500  
501  
502  
503
- Lempe G, Zaunseder S, Wirthgen T, et al (2013) ROI Selection for Remote Photoplethysmography. In: Meinzer HP, Deserno TM, Handels H, et al (eds) *Bildverarbeitung für die Medizin 2013*. Springer Berlin Heidelberg, Berlin, 504  
505  
506

507 Heidelberg, p 99–103

508

509 Li X, Chen J, Zhao G, et al (2014) Remote Heart Rate Measurement from Face  
510 Videos under Realistic Situations. In: 2014 IEEE Conference on Computer  
511 Vision and Pattern Recognition. IEEE, Columbus, OH, USA, pp 4264–  
512 4271, <https://doi.org/10.1109/CVPR.2014.543>, URL <http://ieeexplore.ieee.org/lpdocs/epic03/wrapper.htm?arnumber=6909939>

514

515 Luo H, Yang D, Barszcyk A, et al (2019) Smartphone-Based Blood  
516 Pressure Measurement Using Transdermal Optical Imaging Technol-  
517 ogy. *Circulation: Cardiovascular Imaging* 12(8). [https://doi.org/10.1161/](https://doi.org/10.1161/CIRCIMAGING.119.008857)  
518 [CIRCIMAGING.119.008857](https://doi.org/10.1161/CIRCIMAGING.119.008857), URL [https://www.ahajournals.org/doi/10.](https://www.ahajournals.org/doi/10.1161/CIRCIMAGING.119.008857)  
519 [1161/CIRCIMAGING.119.008857](https://www.ahajournals.org/doi/10.1161/CIRCIMAGING.119.008857)

520

521 Macwan R, Benezeth Y, Mansouri A (2019) Heart rate estimation using remote  
522 photoplethysmography with multi-objective optimization. *Biomedical Signal*  
523 *Processing and Control* 49:24–33. [https://doi.org/10.1016/j.bspc.2018.10.](https://doi.org/10.1016/j.bspc.2018.10.012)  
524 [012](https://doi.org/10.1016/j.bspc.2018.10.012), URL <https://linkinghub.elsevier.com/retrieve/pii/S1746809418302751>

525

526 Nowara EM, McDuff D, Veeraraghavan A (2020) A meta-analysis of the impact  
527 of skin tone and gender on non-contact photoplethysmography measure-  
528 ments. In: *Proceedings of the IEEE/CVF Conference on Computer Vision*  
529 *and Pattern Recognition (CVPR) Workshops*

530

531 Poh MZ, McDuff DJ, Picard RW (2010) Non-contact, automated cardiac  
532 pulse measurements using video imaging and blind source separation. *Optics*  
533 *Express* 18(10):10,762. <https://doi.org/10.1364/OE.18.010762>, URL [https://](https://www.osapublishing.org/abstract.cfm?URI=oe-18-10-10762)  
534 [www.osapublishing.org/abstract.cfm?URI=oe-18-10-10762](https://www.osapublishing.org/abstract.cfm?URI=oe-18-10-10762)

535

536 Rong M, Li K (2021) A multi-type features fusion neural net-  
537 work for blood pressure prediction based on photoplethysmography.  
538 *Biomedical Signal Processing and Control* 68:102,772. [https://doi.org/](https://doi.org/10.1016/j.bspc.2021.102772)  
539 [10.1016/j.bspc.2021.102772](https://doi.org/10.1016/j.bspc.2021.102772), URL [https://linkinghub.elsevier.com/retrieve/](https://linkinghub.elsevier.com/retrieve/pii/S1746809421003694)  
540 [pii/S1746809421003694](https://linkinghub.elsevier.com/retrieve/pii/S1746809421003694)

541

542 Rouast PV, Adam MTP, Chiong R, et al (2018) Remote heart  
543 rate measurement using low-cost RGB face video: a technical litera-  
544 ture review. *Frontiers of Computer Science* 12(5):858–872. [https://doi.](https://doi.org/10.1007/s11704-016-6243-6)  
545 [org/10.1007/s11704-016-6243-6](https://doi.org/10.1007/s11704-016-6243-6), URL [http://link.springer.com/10.1007/](http://link.springer.com/10.1007/s11704-016-6243-6)  
546 [s11704-016-6243-6](http://link.springer.com/10.1007/s11704-016-6243-6)

547

548 Sinhal R, Singh K, Raghuwanshi MM (2020) An Overview of Remote Photo-  
549 plethysmography Methods for Vital Sign Monitoring. In: Gupta M, Konar  
550 D, Bhattacharyya S, et al (eds) *Computer Vision and Machine Intelligence*  
551 *in Medical Image Analysis*, vol 992. Springer Singapore, Singapore, p 21–31

552

553

- Sun Y, Thakor N (2016) Photoplethysmography Revisited: From Contact to Noncontact, From Point to Imaging. *IEEE Transactions on Biomedical Engineering* 63(3):463–477. <https://doi.org/10.1109/TBME.2015.2476337>, URL <http://ieeexplore.ieee.org/document/7268900/>
- Sungjun Kwon, Jeehoon Kim, Dongseok Lee, et al (2015) ROI analysis for remote photoplethysmography on facial video. In: 2015 37th Annual International Conference of the IEEE Engineering in Medicine and Biology Society (EMBC). IEEE, Milan, pp 4938–4941, <https://doi.org/10.1109/EMBC.2015.7319499>, URL <http://ieeexplore.ieee.org/document/7319499/>
- Tominaga S (1994) Dichromatic reflection models for a variety of materials. *Color Research & Application* 19(4):277–285. <https://doi.org/10.1002/col.5080190408>, URL <http://doi.wiley.com/10.1002/col.5080190408>
- Tsouri GR, Kyal S, Dianat S, et al (2012) Constrained independent component analysis approach to nonobtrusive pulse rate measurements. *Journal of Biomedical Optics* 17(7):0770,111. <https://doi.org/10.1117/1.JBO.17.7.077011>
- Tulyakov S, Alameda-Pineda X, Ricci E, et al (2016) Self-Adaptive Matrix Completion for Heart Rate Estimation from Face Videos under Realistic Conditions. In: 2016 IEEE Conference on Computer Vision and Pattern Recognition (CVPR). IEEE, Las Vegas, NV, USA, pp 2396–2404, <https://doi.org/10.1109/CVPR.2016.263>, URL <http://ieeexplore.ieee.org/document/7780632/>
- Verkruyse W, Svaasand LO, Nelson JS (2008) Remote plethysmographic imaging using ambient light. *Optics Express* 16(26):21,434–21,445. <https://doi.org/10.1364/oe.16.021434>
- Wang W, Shan C (2019) Impact of makeup on remote-PPG monitoring. *Biomedical Physics & Engineering Express* <https://doi.org/10.1088/2057-1976/ab51ba>, URL <http://iopscience.iop.org/article/10.1088/2057-1976/ab51ba>
- Wang W, den Brinker AC, Stuijk S, et al (2016a) Algorithmic Principles of Remote PPG. *IEEE Transactions on Biomedical Engineering* 64(7):1479–1491. <https://doi.org/10.1109/TBME.2016.2609282>, URL <http://ieeexplore.ieee.org/document/7565547/>
- Wang W, Stuijk S, de Haan G (2016b) A Novel Algorithm for Remote Photoplethysmography: Spatial Subspace Rotation. *IEEE Transactions on Biomedical Engineering* 63(9):1974–1984. <https://doi.org/10.1109/TBME.2015.2508602>, URL <https://ieeexplore.ieee.org/document/7355301/>

599 Wu BF, Chu YW, Huang PW, et al (2019) Neural Network Based  
600 Luminance Variation Resistant Remote-Photoplethysmography for Driver's  
601 Heart Rate Monitoring. *IEEE Access* 7:57,210–57,225. <https://doi.org/10.1109/ACCESS.2019.2913664>, URL <https://ieeexplore.ieee.org/document/8701432/>  
602  
603  
604

605 Xu S, Sun L, Rohde GK (2014) Robust efficient estimation of heart rate  
606 pulse from video. *Biomedical Optics Express* 5(4):1124. <https://doi.org/10.1364/BOE.5.001124>, URL <https://www.osapublishing.org/boe/abstract.cfm?uri=boe-5-4-1124>  
607  
608  
609

610  
611  
612  
613  
614  
615  
616  
617  
618  
619  
620  
621  
622  
623  
624  
625  
626  
627  
628  
629  
630  
631  
632  
633  
634  
635  
636  
637  
638  
639  
640  
641  
642  
643  
644

[Click here to access/download;Figure;fig.pdf](#) 